Finite Element Analysis of a MEMS-Based High G Inertial Shock Sensor

Y.P. Wang*, R.Q. Hsu*, C.W. Wu**

*Department of Mechanical Engineering, National Chiao Tung University,
1001 Ta-Hsueh Road, 300 Hsinchu, Taiwan, anitawu.wlh@msa.hinet.net
**Department of Mechanical and Mechatronic Engineering, National Taiwan Ocean University
2, Pei-Ning Road, Keelung, Taiwan.

ABSTRACT

Conventional mechanical inertial shock sensors typically use mechanisms such as cantilever beams or axial springs as triggering devices. Reaction time for these conventional shock sensors are either far too slow or, in many cases, fail to function completely for high G (>300G) applications.

In this study, a Micro-Electro-Mechanical (MEMS)-based high G inertial shock sensor with a measurement range of 3,000–21,000 G is presented. The triggering mechanism is a combination of cantilever and spring structure. The design of the mechanism underwent a series of analyses. Simulation results indicated that a MEMS-based high G inertial shock sensor has a faster reaction time than conventional G inertial shock sensors that use a cantilever beam or spring mechanism.

Furthermore, the MEMS-based high G inertial shock sensor is sufficiently robust to survive the impact encountered in high G application where most conventional G inertial shock sensors fail.

Keywords: MEMS, high G, inertial shock sensor, spring, proof mass.

1 INTRODUCTION

Inertial sensors have been extensively utilized in science and industry. For high G (>300G) applications, reaction times for conventional mechanical type shock sensors are not fast enough. In some cases the shock sensor structures disintegrate (>5000G). Designing a shock sensor that has a faster reaction time than conventional sensors and a mechanism that is sufficiently robust to survive the impact when a vehicle collides with a hard target is the major goal of this study. Thus, a MEMS high-G inertial shock sensor that has two advantages is presented. Silicon was first chosen as the structure material, as its Young's modulus [1] approaching 190 Gpa, which is close to that of steel (210 Gpa). Moreover, silicon has virtually no mechanical hysteresis, and, thus, is an ideal material for sensors and actuators.

Second, the MEMS process favors production of miniature mechanisms that are always demanding in the application. Trimmer [2] proposed a unique model that demonstrated reducing the scale of a structure, will decrease the time required for displacing a fixed point. Thus, the reaction time of a small inertial shock sensor can be decreased.

2 THEORETICAL ANALYSIS

Fig. 1 presents the proposed micro shock sensor. This sensor uses a Mass-Damper-Spring Dynamic (MDS) System to trigger the mechanism.

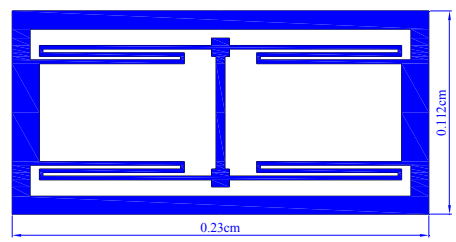

Fig. 1 The micro shock sensor proposed in this study

Fig. 2 is a schematic of the system. The dynamic equation of motion of proof mass can be expressed by one-dimensional lumped-system model given by [3]

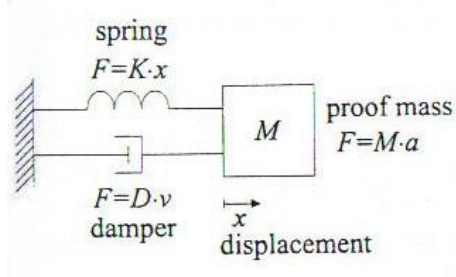

Fig. 2 Mass-Spring-Damping System

$$M\frac{d^2x}{dt^2}+D\frac{dx}{dt}+Kx=F_{ext}=Ma \qquad (1)$$

where F_{ext} is the external force acting on the frame, D is the damping factor, K is the effective spring constant of the elements and M is the proof mass attached to a fixed frame by one or more spring elements. Using the Laplace transformation, the following second-order function for acceleration of the mass is

$$H(s)=\frac{X(s)}{A(s)}=\frac{1}{s^2+\frac{D}{M}s+\frac{K}{M}}=\frac{1}{s^2+\frac{w_r}{Q}s+w_r^{\ 2}} \qquad (2)$$

where $w_r=\sqrt{\frac{K}{M}}$ is the resonance frequency and Ms= $\frac{M}{K}$ is the mechanical sensitivity of the system. Thus, system mechanical sensitivity varies with the spring constant and proof mass. Reducing the spring constant or increasing proof mass, increases mechanical sensitivity and shortens reaction time.

3 FINITE-ELEMENT SIMULATION

The spring is divided into four sections and anchored on two sides of the sensor frame structure. The proof mass is located at middle zone of the sensor and linked with the four spring sections. To evaluate system reaction time, 10 different arrangements of spring and proof mass were tested. All proof masses have the same thickness; consequently, the ratio of these masses is equal the ratio of proof mass surface areas. We assume that the proof mass scale in type 4 is 1.0. Fig. 3 presents the different sensor designs considered in this study.

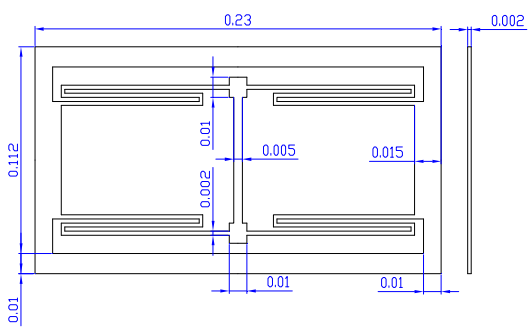

（a）Type 1 （cm）

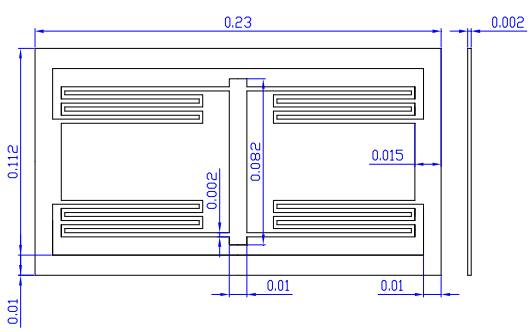

（b）Type 4 （cm）

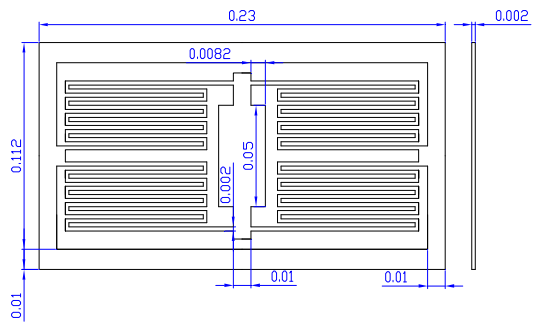

（c）Type 10 （cm）

Fig. 3 Diagrams and dimensions of 4 typical sensors

Table 1 presents their proof masses and coil numbers. Finite element analyses for displacement of the proof mass when the sensor encountered an impact were performed with ANSYS version 8.0 and LS-DYNA [4]. The mesh element adopted for modeling the proposed sensors is type SOLID 164 that is used for 3-D modeling of solid structures and defined by eight nodes with six degrees of freedom at each node, namely, translations, velocities, and accelerations in nodal directions x, y, and z. Only one-half of the sensors were utilized for simulation because of the symmetricity of sensor's form. Fig. 4 shows typical finite element meshes for a spring and proof mass. Table 2 lists the number of nodes and elements in each sensor.

Sensor type	Proof mass scale	Coil number
1	0.62	4
2	1.0	4
3	0.62	8
4	1.0	8
5	0.62	12
6	1.0	12
7	2.24	12
8	0.62	16
9	1.0	16
10	2.24	16

Table 1 The proof mass scale & coil number of the sensor

The spring and proof mass are assumed to be made of silicon, with a modulus of elasticity of 190 GPa, Poisson's ratio of 0.23 and density of 2.3g/cm3. Other assumptions are as follows: (a) the enclosure frame of the sensor is a rigid body; (b) the dimensions of sensor components are sufficiently large for principles of continuum mechanics that are applicable for analysis [5]; and, (c) the air damping effect can be ignored as the shock sensor is packaged in a vacuum environment.

Because of the complication of the spring shape, a direct calculation of the spring constant K is almost impossible. Instead, we use ANSYS to simulate the proof mass

displacement under various load. Fig. 5 is an example of the simulation result of the proof mass displacement under load. Fig. 6 is a depiction of the displacement / applied force for type 1-10 sensors. Apparently, $K_1 = K_2 > K_3 = K_4 > K_5 = K_6 = K_7 > K_8 = K_9 = K_{10}$.

In simulation, a series of half-sine waves were applied to sensors. Seven different G values, ranging from 3,000–21,000G, are considered in the simulation in accordance with (Mil-Std-810F) [6].

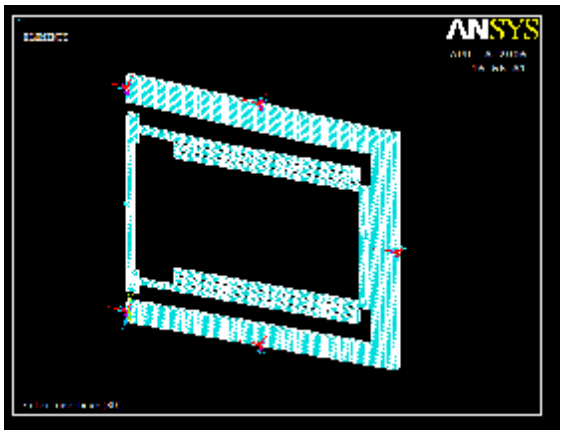

Fig. 4 The finite element meshes of the type 1 sensor

Sensor type	Node number	Element number
1	17100	9518
2	17676	9908
3	19833	10684
4	20373	11050
5	22524	11822
6	23085	12202
7	24159	12900
8	25245	12980
9	25833	13378
10	27003	14140

Table 2 The number of the nodes and elements

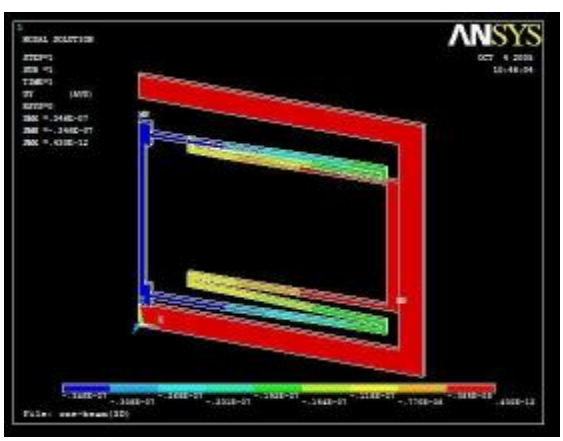

Fig. 5 Proof mass displacement of the type 1 sensor

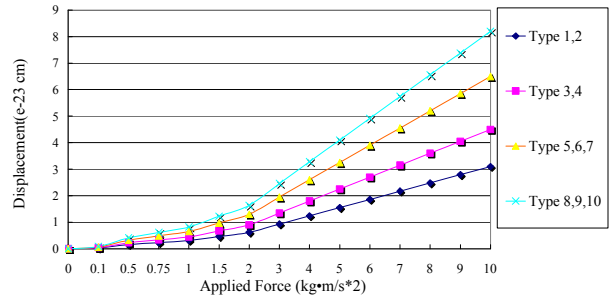

Fig. 6 Displacement vs. applied forces for each sensor

4 RESULTS AND DISCUSSION

In the dynamic simulations of time-domain analysis, a shock wave (G–T curve) is loaded onto an impact sensor, and the responses of the impact sensor are identified by observing the displacement of the proof mass in the impact direction. When the proof mass contacts the top frame (the displacement is 5.0E-03 cm), the impact sensor triggers. When the proof mass does not reach the top frame, the sensor does not trigger.

Simulation results demonstrated that the spring constant was reduced or proof mass increased, the G value required for the sensor to trigger and response time decreased (Table 3).

Two principal categories of reaction times were identified. First, when a proof mass increases from 0.62 to 2.24, and the spring constant remains unchanged, the reaction time is decreased (Fig. 7) and the minimum triggering G value decreases for sensors (Fig. 8). Second, reducing the spring constant, and retaining the proof mass, the reaction time decreased (Fig. 9) and the trigger G value decreased for sensors (Fig. 10).

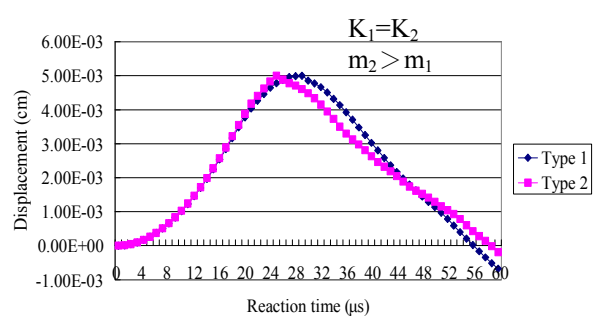

Fig. 7 Reaction time of the sensors at 21000G

G value / Sensor type	21000	20000	10000	8000	5000	4000	3000
1 (m1 0.62 , K_1)	28.9	×	×	×	×	×	×
2 (m2 1.0 , K_2)	24.9	25.9	×	×	×	×	×
3 (m3 0.62 , K_3)	21.9	23.9	34.9	×	×	×	×
4 (m4 1.0 , K_4)	21.9	22.9	33.9	40.9	×	×	×
5 (m5 0.62 , K_5)	21.9	22.9	31.9	35.9	52.9	×	×
6 (m6 1.0 , K_6)	21.9	22.9	31.9	35.9	48.9	×	×
7 (m7 2.24 , K_7)	21.9	22.9	31.9	35.9	47.9	56.9	×
8 (m8 0.62 , K_8)	21.9	22.9	31.9	35.9	46.9	52.9	×
9 (m9 1.0 , K_9)	21.9	22.9	31.9	35.9	45.9	51.9	×
10 (m10 2.24,K_{10})	21.9	22.9	31.9	35.9	44.9	50.9	65.9

Table 3 The response time (μ s) of the micro-sensors

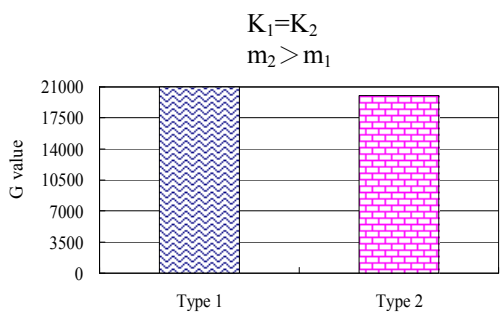

Fig. 8 Minimum G values for the sensors to be triggered

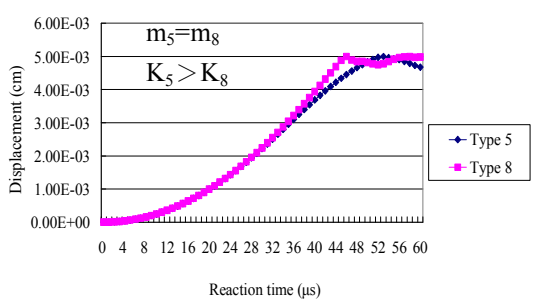

Fig. 9 Reaction time of the sensors at 5000G

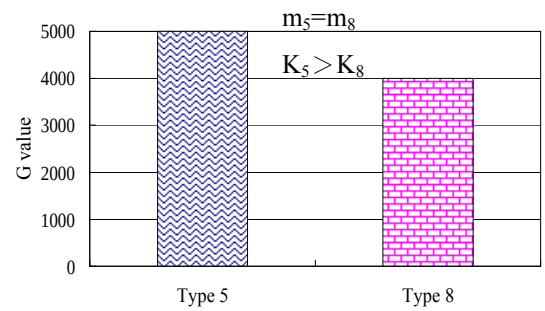

Fig. 10 Minimum G values for the sensors to be triggered

5 CONCLUSION

This proposed shock sensor is intended for use at 3,000–21,000G. Ten different designs were analyzed. Simulation results demonstrated that these MEMS high G inertial shock sensors have faster reaction times than conventional G inertial shock sensors. The shock sensors were sufficiently robust to survive the impact of at least 21,000G, four times higher than that of conventional inertial shock sensors.

REFERENCES

[1]. Donald R. Ask eland, The science and engineering of materials, 1st edn, Taipei, Kai Fa, 1985, ch. 6, pp. 126-127.

[2]. Trimmer, W.S.N, Microrobots and Micromechanical Systems, Sensors and Actuators vol.19 no.3, pp. 267-287, 1989.

[3]. M. Elwenspoek, R. Wiegerink, Mechanical Microsensors, Germany, Springer, 2001.

[4]. Training Manual, Explicit Dynamics with ANSYS/LS-DYNA, 1st edn, U.S.A, SAS IP, 2001.

[5]. Tai-Ran Hsu, MEMS & Microsystems Design and Manufacture, international edition 2002, Singapore, McGraw-Hill, pp. 157-159.

[6]. Military Standard, Mechanical Shock Test, MIL-STD-883E Method 2002.4, US Dept. of Defense, 2004.